Article:
Sun, Y, Zhang, P, Wang, X et al. (3 more authors) (2022) Deciphering key coloured compounds from sunless tanning reactions. Dyes and Pigments, 204. 110448. ISSN 0143-7208

https://doi.org/10.1016/j.dyepig.2022.110448

Deciphering key coloured compounds from sunless tanning reactions

Yufa Sun[a], Peiyu Zhang[b], Xingyu Wang[b], Fatimah A. M. Al-Zahrani[c,a], Nora H. de Leeuw[b] and Long Lin[a,*]

[a] Colour Science, School of Chemistry, University of Leeds, Woodhouse Lane, Leeds LS2 9JT, UK
[b] School of Chemistry, University of Leeds, Woodhouse Lane, Leeds LS2 9JT, UK
[c] Chemistry Department, Faculty of Science, King Khalid University, P.O.Box 9004, Abha 61413, Saudi Arabia
*Corresponding author; e-mail address: l.lin@leeds.ac.uk

KEYWORDS: Dihydroxyacetone; sunless tanning; Maillard reaction; colour dilution analysis; coloured compounds

ABSTRACT: Sunless tanning has become an incredibly popular way to achieve a tanned look without the potential skin damage from sun exposure, due to its convenience and safety compared to the conventional solar tanning. Dihydroxyacetone (DHA), as the main active ingredient in commercial sunless tanning products, is widely recognized to react with free amino acids (AAs) in the outer stratum corneum of skin to form brown pigments known as "melanoidins" through the Maillard reaction. However, the exact reaction pathways and chemical structures of the melanoidins formed have not yet been reported. To explore the colour development mechanism of DHA, three typical AAs, i.e. arginine, histidine and lysine, were each made to react with DHA using a simplified model system. For the first time, three key coloured compounds with the same chromophore were successfully isolated and identified from these resultant mixtures. The reaction pathway for the formation of these key coloured compounds was also proposed and the associated energy calculated using the methods based on the density functional theory (DFT). In addition, an in-depth understanding of the colour properties of these key coloured compounds has been gained through the colour dilution analysis for their colour contributions and by using *CIELAB* colour space to evaluate their colour characteristics, respectively.

1. INTRODUCTION

The Maillard reaction, also known as the nonenzymatic browning reaction, is a complex chemical reaction that occurs via the condensation of carbonyl groups on reducing sugars with amino groups on amino acids (AAs), peptides and proteins [1],[2]. The reaction was discovered in 1921 by French chemist Louis-Camile Maillard and its mechanism was detailed in 1951 by American chemist John E. Hodge, who proposed a scheme including three stages and eight types of reaction [3]. Colour formation is the most obvious and basic features of the Maillard reaction [4]. The coloured compounds generated by the Maillard reaction can be divided into two classes, based on their molecular weight, namely low-molecular-mass coloured compounds and high molecular weight melanoidins (>1000 Da) [5],[6]. Despite extensive studies, especially in food, such as the cooking of meat, roasting of coffee and baking of bread, surprisingly little is known about the chemical structures responsible for the typical brown colour, due to the complexity and multiplicity

of the Maillard reaction products formed [7]. Therefore, suitable model systems have been investigated to obtain more detailed information on the structures of the chromophoric compounds involved in the reaction.

In the 1960s and 1970s, the Maillard reaction took a center stage when it became the basis for the operation of sunless tanning products [8]. Tanning has since become an incredibly popular activity in Western countries, especially for young people, as a tanned skin is usually perceived as attractive and healthy [9]. Dihydroxyacetone (DHA), a three-carbon sugar, is the main active ingredient in commercial sunless tanning products [10],[11]. The first to discover the browning of skin from DHA and its connection with the browning in food was Eva Wittgenstein, by accident, when she used DHA as an oral drug to assist children with glycogen storage disease in 1960 [12]. She suggested that the carbonyl group of DHA reacted with the amino groups of AAs derived from epidermal proteins of skin via the Maillard reaction to form brown pigments [13]. Soon after, the first commercial self-tanning product was developed and launched, which immediately achieved great success. To date, DHA is the only legal tanning agent approved by the US Food and Drug Administration (FDA) for external application in cosmetic products [9]. Meanwhile, due to its popularity and commercial value, the roles of DHA in the tanning reactions of skin have attracted considerable research attention [14]. Many researchers have developed some good adjuvants, such as methionine sulphoxide, perfluoropolyether phosphate and ethylenediamine derivatives, to increase the stability of DHA and its rate of tanning [15],[16],[17]. In addition, there have been a number of observations of free radicals being involved in the production of DHA-induced melanoidins in skin[18],[19]. However, despite extensive studies over the past 60 years, knowledge of the exact reaction pathways and chemical structures of melanoidins still remains rather rudimentary.

To better understand the colour development of DHA, it is necessary to study the tanning reaction within suitable chemically constituted model systems rather than in natural skins which are invariably chemically complex [20]. In our previous study, the colour development of the Maillard reaction between three typical AAs (arginine, histidine and lysine) and DHA has been systematically investigated under various reaction conditions [21]. Based on the optimised reaction conditions, the study reported here focused on exploring the chemical structure of the key coloured compounds formed in these model reactions, and explaining their relationship between their colour and the structure. These key coloured compounds were first isolated and purified using preparative high performance liquid chromatography (HPLC), then analysed and determined by the ultraviolet-visible spectroscopy (UV-Vis), fourier-transform infrared spectroscopy (FT-IR), high resolution mass spectroscopy (HR-MS) and one-, two-dimensional nuclear magnetic resonance spectroscopy (1D and 2D-NMR). To the best of our knowledge, these identified compounds have not as yet been reported in the literature. Based on the chemical information obtained, the mechanism of formation of the key coloured compound was proposed and calculated using the density functional theory (DFT) methods. In addition, the colour dilution analysis (CDA) was used to evaluate the colour contributions of these compounds to the colour of the reaction mixtures and *CIE LAB* colour space was used to further evaluate their colour characteristics. These findings not only provide a foundation for further study of the chemical structure of melanoidins on real human skin, but it can also be utilized to improve the tanning effect of DHA more safely and efficiently.

2. EXPERIMENTAL SECTION

2.1 Chemicals

Dihydroxyacetone (DHA) was supplied by PZ Cussons (Manchester, England). L-Arginine hydrochloride (Arg), L-Histidine hydrochloride (His) and L-Lysine hydrochloride (Lys) were purchased from Ajinomoto Inc and used without further purification. HPLC-grade acetonitrile was supplied by Merck Life Science UK Limited. Hydrochloric acid, sodium acetate and acetic acid were supplied by Sigma-Aldrich Corporation.

2.2 Preparation of model systems (AA-DHA)

The three model reaction solutions were prepared and denoted as Arg-DHA, His-DHA and Lys-DHA, respectively. Based on the optimised reaction conditions obtained from previous study, each reaction solution was dissolved into 20 mL 0.1 M acetate buffer solution of pH 5.6 in a sealed tube at 50 °C for 72 hours, respectively, as shown in Table S1.

2.3 High performance liquid chromatography (HPLC)

Analytical HPLC with diode array detection (DAD) was carried out using a reverse-phase C_{18} column and a water-acetonitrile gradient (acetonitrile: 5 ~ 95%, 5 min, 254 nm as signal). These mixtures were separated and purified on the preparative mass directed-HPLC (Agilent Technologies, 1290 Infinity) with a Kinetex EVO C_{18} column (21.2 × 250 mm, 5 μm, 100 Å). The separation conditions are as follows: injection volume was 900 μL, flow rate was 10 mL/min, gradient started with a mixture of water-acetonitrile (95:5, v/v), then acetonitrile content was increased to 20% within 20 min. The chosen wavelength for detection was 254 nm. Time-based detector method (0.6 min) was used to collect the key coloured compounds. For each run, only a small amount of sample (~0.6 mg) was collected. Multiple times for the repeated run were required to obtain sufficient amounts of sample for NMR. The collected compounds were lyophilised on a freeze-dryer, equipped with an Edwards two stage vacuum pump using 50 mL poly(styrene) falcon tubes.

2.4 Ultraviolet-visible spectroscopy (UV-Vis)

UV-Vis absorption spectrum of samples were performed on a dual beam Varian Cary 50 UV-Vis spectrophotometer (Agilent Technologies), equipped with a xenon pulse lamp and scan software. Samples were analysed in a quartz cuvette (10 mm, QS, Hellma) at a concentration of 3 mmol/L (~1 mg/mL). The absorbance at 420 nm was used to evaluate the browning intensity of Maillard mixtures.

2.5 Fourier-transform infrared spectroscopy (FT-IR)

FT-IR spectrometry was recorded via a Bruker ALPHA-P FT-IR spectrometer, equipped with Bruker OPUS 7.0 software and a diamond attenuated total reflectance (ATR) accessory. Spectra were collected between 4000 cm^{-1} and 500 cm^{-1}, accumulated over 100 runs.

2.6 High resolution mass spectroscopy (HR-MS)

The accurate molecule mass, to four decimal places, of each of the samples was performed on a Bruker MaXis Impact using the positive electrospray ionization (ESI). The sample was diluted to 1 mg/mL in water based on the mass concentration of the reactants. The scan range was from 50 to 1500 m/z. The spectra were recorded in the Bruker Compass Data Analysis 4.3, to determine the accurate molecular mass and chemical formula.

2.7 Nuclear magnetic resonance spectroscopy (NMR)

Proton (^{1}H), carbon (^{13}C), distortionless enhancement by polarization transfer (DEPT-135), heteronuclear single-quantum correlation spectroscopy (^{1}H-^{13}C HSQC) and heteronuclear multiple-bond correlation spectroscopy (^{1}H-^{13}C HMBC) experiments were performed on a Brucker Avance 500 MHz spectrometer fitted with a 5 mm Bruker C/H cryoprobe. Chemical shifts (δ) in ppm were referred to a trimethylsilane (TMS) standard whose chemical shift is 0 ppm. NMR spectra were analysed using MestreNova® Research Lab software. NMR data were recorded as follows: δ [multiplicity, coupling constant (J, Hz), relative integral], where multiplicity was defined as s = singlet, d = doublet, t = triplet, q =

quartet, m = multiplet. The signal due to residual D_2O appearing at δ_H 4.80 was used to reference ^1H and ^1H-^{13}C NMR spectra, respectively.

2.8 Density functional theory (DFT)

All calculations were performed using the density functional theory (DFT) method in the Gaussian 09W program [22]. The Gauss View 05 visualization program was used to input and output the molecular structures. All geometries were optimised using the hybrid functional B3LYP at 6-311+ basis set in water solution via the polarization continuum model (PCM), and to validate the optimised stationary point, frequencies were also calculated at this level. In addition, all calculations would get converged if the gradient forces were smaller than a threshold value of 0.00045 Hartree (1 Hartree = 27.211 eV). Changes in the Gibbs Free Energy (ΔG) were calculated as shown in Equation 1:

$$\Delta G = G_{product} - G_{reactant} \quad (1)$$

2.9 Colour characterization

2.9.1 Molar extinction coefficient (ε)

The molar extinction coefficient (ε) at its maximum absorption wavelength (λ_{max}) is a useful method to evaluate the colour intensity or strength of a colourant, especially for a series of colourants if their curves have similar shape [23]. It can be calculated from the UV-Vis absorption spectrum of a colourant in solution at low concentration using the Beer-Lambert-Law (Equation 2) [24]:

$$A = \varepsilon cl \quad (2)$$

Where A is the absorbance of a colourant at a particular wavelength (λ_{max}), c is the concentration of a colourant and l is the pathlength of the cell (commonly 1 cm) used for the measurement.

2.9.2 Colour dilution factor (CDF)

The resultant Maillard mixtures were repeatedly diluted with respective solvents until their absorbance values at 420 nm were the same as those of the solvents (water in this study). Using this procedure, a colour dilution factor (CDF_{total}) was defined for each reaction mixture.

2.9.3 Colour detection threshold (CDT)

A solution, containing a known amount of the colourant, was diluted with its colourless solvent until no colour difference from the solvent could be instrumentally detected at 420 nm. The concentration of the colourant, at this point, was defined as the colour detection threshold (CDT).

2.9.4 Colour activity value (CAV) and colour contribution (CC)

To evaluate the colour impact of a single coloured reaction product, Hofmann has made a crucial step by defining a colour activity value (CAV) and colour contribution (CC) [25]. CAVx is the ratio of the concentration of a colourant x to its detection threshold (Equation 3). The colour contribution of a component colourant x (CCx) to the colour of the total Maillard mixture, which was defined as 100% colour activity, was calculated as follows (Equation 3):

$$\mathrm{CAV}x = \frac{\text{Concentration}x\ (\text{mmol/L})}{\text{Detection threshold}x\ (\text{mmol/L})} \qquad \mathrm{CC}x = \frac{\mathrm{CAV}x}{\mathrm{CDFtotal}} \times 100\% \quad (3)$$

2.9.5 CIE colour space

The colour of each sample was characterised by *CIE L*a*b** (*CIELAB*), which is a colour space defined by the International Commission on Illumination (*CIE*) in 1976 [26]. It expresses colour as three primary values: L^* for the lightness from black (0) to white (100), a^* from green (−) to red (+), and b^* from blue (−) to yellow (+), plus where secondary values for chroma (C^*) and hue (h) can be represented by Equation 4:

$$C^* = \sqrt{a^{*2} + b^{*2}} \qquad h = arctan\frac{b^*}{a^*} \quad (4)$$

Colour measurement performed in this study involved pipetting the sample aliquot into a 1 cm polymethyl methacrylate (PMMA) plastic cuvette, and measuring the *L*a*b** values of the sample against a white background using a Datacolor CHECK 3 (Datacolor Inc., UK), with an 8° diffuse D65 illuminant and at a 10° observer angle, calibrated using a standard white and black plate. Each test was carried out in triplicate and the mean value is reported.

3. RESULTS and DISCUSSION

It is widely accepted that the second stage of the Maillard reaction can generate a tremendous variety of reactive compounds, such as ketones, aldehydes, dicarbonyls and heterocyclic compounds, via dehydration, fragmentation, Strecker degradation and cyclisation [2],[27],[28]. The large variety of these intermediates then undergo a complex reaction in the final stage, not only leading to the multiplicity and the low yields of the coloured compounds, but also making their isolation and identification a significant challenge. Therefore, it is almost impossible to isolate and identify all coloured compounds formed in the complex Maillard mixture. To characterize the key chromophores, a screened process was first used to select the key coloured compounds from AA-DHA, followed by their identification and the discussion of their formation mechanism. Finally, the colour contribution and characteristic of these key coloured compounds were further evaluated quantitatively, aimed at establishing the structure-colour relationship and exploring the colour difference in AA-DHA systems.

3.1 Screening for the key coloured compounds in AA-DHA

The resultant solutions of L-arginine, histidine and lysine with DHA were coded Arg-DHA, His-DHA and Lys-DHA, respectively. The reaction of DHA with AAs in water at 50 °C resulted in a series of colour changes: yellow, then red and finally dark brown. To quantitatively study the total colour intensity of the Maillard mixtures, a colour dilution factor (CDF) was used, for the first time in this study, to evaluate the browning intensity of these mixtures. As shown in Table 1, His-DHA has the highest CDF value with 864, followed by Lys-DHA with 816, whereas a very low CDF of 174 was determined for Arg-DHA, which was consistent with the observed colour difference (Figure 1). Analytical HPLC results of these mixtures revealed that there were 7, 14 and 11 peaks in the chromatograms for Arg-, His- and Lys-DHA reaction mixtures, respectively (Figure S1 ~ S3). Although different coloured compounds were formed in the reactions, the main coloured compounds in the three mixtures appeared to have similar retention times. It can be seen clearly from these chromatograms that these peaks at 0.66 min (labelled **A1**), 0.64 min (labelled **H1**) and 0.65 min (labelled **L1**) were due to the main products and at 254 nm accounted for around 47%, 41% and 38% in Arg-, His- and Lys-DHA, respectively. The following experiments were then focused on the structural identification of these key colourants.

Table 1. CDF of AA-DHA and contents of the key colourants in AA-DHA

Maillard mixture	CDF_{total}	Content in AA-DHA (%)		
		A1	**H1**	**L1**
Arg-DHA	174	47	—	—
His-DHA	864	—	41	—
Lys-DHA	816	—	—	38

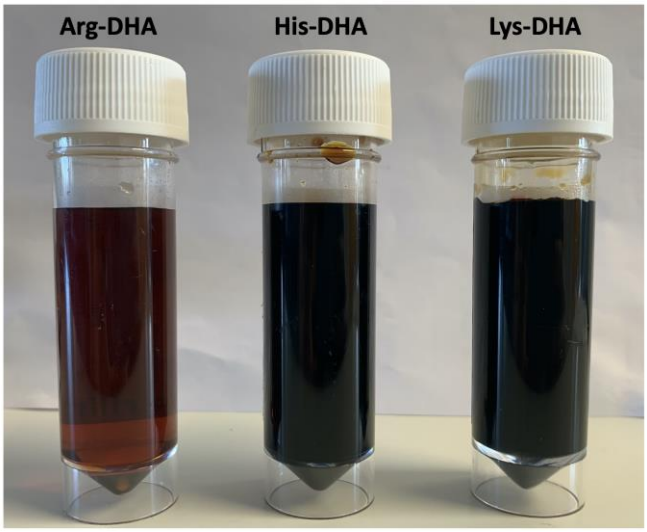

Figure 1. Images of AA-DHA mixtures obtained under the optimised reaction conditions (72 hours, pH 5.6, 50 °C)

3.2 Identification of the key coloured compounds in AA-DHA

Three key coloured compounds (Colourants **A1**, **H1** and **L1**) were isolated from the AA-DHA mixtures using mass-directed preparative HPLC and their chemical structures are shown in Figure 2a. Due to having the same chromophore, they showed similar curves with an absorption maximum at 266 nm in water (Figure 2b). Although the colour of their solution is all yellow, their colour intensities were different. According to the Beer-Lamber Law, the calculated ε values of **A1**, **H1**, and L1 were 257, 393, and 360 $L \cdot mol^{-1} \cdot cm^{-1}$, respectively, which can be used to explain the difference in the colour intensity. In addition, it can be seen from Figure 2c that **A1**, **H1**, and **L1** all exhibited some similar characteristic absorption peaks. The peaks at 2930, 1378, 1216, and 1092 cm^{-1} were assigned to the C-H stretching of alkane, C-H bending of alkane, C-N stretching, and C-O stretching vibrations, respectively, which illustrated the presence of the corresponding AA moieties [29]. Besides, compared with the DHA and original AAs (Figures S5, S13, and S21), many new characteristic absorption peaks appearing at 3140, 1712, and 1607 cm^{-1} were assigned to the C-H stretching vibration of alkene, C=O stretching vibration, and C=C stretching vibration of unsaturated ketone, respectively [30]. Meanwhile, the peaks at 914, 820, and 769 cm^{-1} were resulted from the C=C bending vibrations. The appearance of these new peaks was consistent with the characteristic groups contained in the key chromophore of **A1**, **H1**, and **L1**. The detailed process for the exact structure determination using MS and NMR was described in the following sections [31].

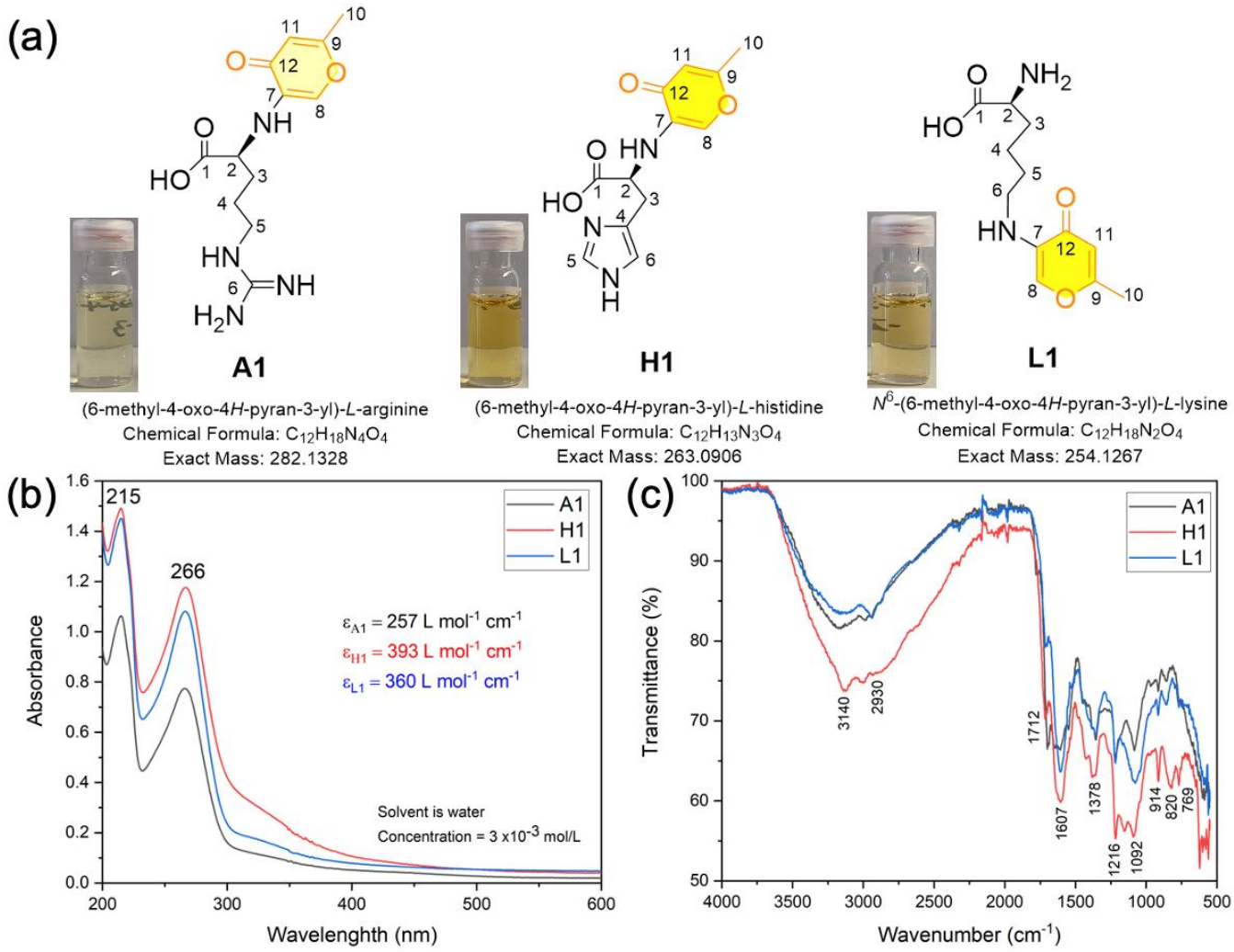

Figure 2. (a) Chemical structures (b) UV-Vis (c) FT-IR of Colourants **A1**, **H1**, and **L1**

Colourant **A1**. Colourant **A1** was isolated and purified from Arg-DHA as a light-yellow solid. Its 254 nm analytical HPLC chromatogram showed a peak with a retention time of 0.35 min (Figure S4), whose purity was ~89% at 254 nm. Results from the electrospray ionisation (ESI) of LC-MS indicated that this compound generated an $[M + H]^+$ ion at m/z 282.94, as well as fragment ions at m/z 126.62 (Figure S6). HR-MS also showed an $[M + H]^+$ peak at 283.1396, and confirmed the target compound to have a molecular formula of $C_{12}H_{18}N_4O_4$, which is the dehydration product of Arg and two DHA after the loss of four water molecules. The ^{1}H-NMR spectrum showed 7 resonance signals (Figure S7) and the corresponding NMR data are given in Table S2. The chemical shifts of signals at 3.99 [m, 1H, H-C(2)], 3.25 [t, J = 6.9 Hz, 2H, H-C(5)], 1.96 [d, J = 1.1 Hz, 2H, H-C(3)] and 1.74 [m, 2H, H-C(4)] confirmed the presence of the Arg moiety in **A1**. The singlets at 8.03 [s, 1H, H-C(8)] and 6.40 [s, 1H, H-C(11)] were in the chemical shift range of hydrogens on the non-adjacent olefins. The chemical shift at 2.34 [s, 3H, H-C(10)] was the characteristic signal of hydrogen on the methyl ($-CH_3$). The ^{13}C-NMR spectrum (Figure S8) showed signals of 12 different carbon atoms. DEPT-135 experiment (Figure S9) revealed that 3 and 4 of the 12 signals corresponded to the secondary ($-CH_2$) and the primary ($-CH_3$) or the tertiary (-CH) carbon atoms, respectively. Their specific correlations between a carbon and its attached protons were further confirmed by the HSQC (Figure S10). The remaining 5 signals were the quaternary carbon atoms. Unequivocal assignment of these carbon atoms could be successfully achieved by means of HMBC (Figure S11).

Colourant **H1**. Colourant **H1** was isolated and purified from His-DHA as a yellow solid. Its 254 nm analytical HPLC chromatogram showed a peak with a retention time of 0.33 min (Figure S12), whose purity was ~81% at 254 nm. Results from ESI of LC-MS indicated that this compound generated an $[M + H]^+$ ion at m/z 263.86, as well as fragment ions at m/z 126.66 (Figure S14). HR-MS also showed an $[M + H]^+$ peak at 264.0982, and confirmed the target compound to have a molecular formula of $C_{12}H_{13}N_3O_4$, which is the dehydration product of His and two DHA after the loss of four water molecules. The ^{1}H-NMR spectrum showed 7 resonance signals (Figure S15) and the corresponding NMR data are given in Table S4. The chemical shifts of signals at 8.60 [s, 1H, H-C(6)], 7.43 [s, 1H, H-C(5)], 4.24 [m, 1H, H-C(2)] and 3.42 [t, *J* = 6.2 Hz, 2H, H-C(3)] confirmed the presence of the His moiety in the Colourant **H1**. The singlets at 8.01 [s, 1H, H-C(8)] and 6.38 [s, 1H, H-C(11)] were in the chemical shift range of hydrogens on the non-adjacent olefins. The chemical shift at 2.33 [s, 3H, H-C(10)] was the characteristic signal of hydrogen on the methyl ($-CH_3$). These characteristic signals were similar to those of **A1**. The ^{13}C-NMR spectrum (Figure S16) showed signals of 12 different carbon atoms. DEPT-135 experiment (Figure S17) revealed that 1 and 6 of the 12 signals corresponded to the secondary ($-CH_2$) and the primary ($-CH_3$) or the tertiary (-CH) carbon atoms, respectively. Their specific correlations between a carbon and its attached protons were further confirmed by the HSQC (Figure S18). The remaining 5 signals were the quaternary carbon atoms. Unequivocal assignment of these carbon atoms could be successfully achieved by means of HMBC (Figure S19). All ^{13}C NMR signals are summarised in the Table S5.

Colourant **L1**. Colourant **L1** was isolated and purified from Lys-DHA as a yellow solid. Its 254 nm analytical HPLC chromatogram showed a peak having a retention time of 0.31 min (Figure S20), whose was ~82% at 254 nm. Results from ESI of LC-MS indicated that this compound generated an $[M + H]^+$ ion at m/z 254.89, as well as fragment ions at m/z 126.89 (Figure S22). HR-MS also showed an $[M + H]^+$ peak at 255.1343, and confirmed the target compound to have a molecular formula of $C_{12}H_{18}N_2O_4$, which is the dehydration product of Lys and two DHA after the loss of four water molecules. The ^{1}H-NMR spectrum showed 8 resonance signals (Figure S23) and the corresponding NMR data are given in Table S6. The chemical shifts of signals at 3.77 [dd, J = 12.0, 8.5 Hz, 1H, H-C(2)], 3.02 [m, 2H, H-C(6)], 1.90 [m, 2H, H-C(3)], 1.71 [m, 2H, H-C(5)] and 1.40 [m, 2H, H-C(4)] confirmed the presence of the Lys moiety in the Colourant **L1**. The singlets at 8.03 [s, 1H, H-C(8)] and 6.40 [s, 1H, H-C(11)] were in the chemical shift range of hydrogens on the non-adjacent olefins. The chemical shift at 2.34 [s, 3H, H-C(10)] was the characteristic signal of hydrogen on the methyl ($-CH_3$). These characteristic signals were similar to those of **A1** and **H1**. The ^{13}C-NMR spectrum (Figure S24) showed signals of 12 different carbon atoms. The DEPT-135 experiment (Figure S25) revealed that 4 each of the 12 signals corresponded to the secondary ($-CH_2$) and the primary ($-CH_3$) or the tertiary (-CH) carbon atoms, respectively. Their specific correlations between a carbon and its attached protons were further confirmed by the HSQC (Figure S26). The remaining 4 signals were the quaternary carbon atoms. Unequivocal assignment of these carbon atoms could be successfully achieved by means of HMBC (Figure S27). All ^{13}C NMR signals are summarised in the Table S7. In summary, these obtained spectroscopical data were consistent with the proposed structure of **A1**, **H1** and **L1** (Figure 2).

3.3 Reaction pathways for the key colourants in AA-DHA

On the basis of the experimental data, the reaction pathway leading to the formation of the key coloured compounds in AA-DHA has been proposed and is shown in Figure 3. One fact that has been widely accepted is that the Maillard reaction starts with the condensation of the carbonyl group of DHA with the free (unprotected) amino group of an amino acid, followed by dehydration resulting in the formation of a Schiff base (**4**). Then, the unstable Schiff base undergoes Amadori rearrangement to give a Heyns product (**5**) [20]. Meanwhile, methylglyoxal (MGO) can be formed by DHA

under the catalysis of acid or base, which plays the important role as a precursor of aroma and colour compounds in the Maillard reaction, especially in Strecker degradation, which is a key flavour-generation reaction [32],[33]. Since MGO has a significantly higher reactivity than DHA, it further reacts with the Heyns product via aldol reaction to form **6**. Tautomerisation of **6** would generate the enol and its E-form could cyclise in a 6-exo-trig process to generate **7** [30]. Finally, dehydration leads to the formation of the key coloured compound **8**, which has a conjugated double-bond structure. It corresponds to **A1**, **H1** and **L1** in the Arg-, His- and Lys-DHA, respectively.

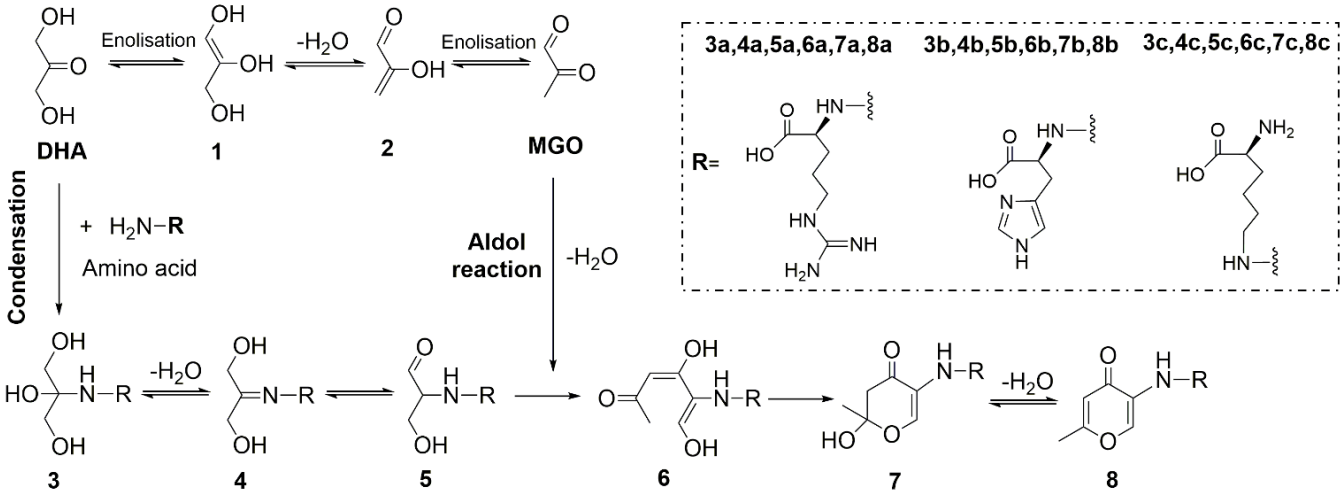

Figure 3. Proposed reaction pathways for the formation of key coloured compounds in AA-DHA

To further prove the rationality of the proposed reaction mechanisms, the pathways to these compounds were calculated using the Gaussian 09W program package, which is based on the density functional theory (DFT) [34],[35]. The details of the calculated energies and all optimised structures are summarised in Table S8 and Figure S28 ~ 30, respectively. It can be clearly seen from Figure 4 that the formation of **3a**, **3b** and **3c** is endothermic costing 0.36, 0.58, and 0.53 eV, respectively, with respect to the initial reactants. However, there is a significant difference in the formation of Schiff base between Arg-, His- and Lys-DHA. The formation of **4a** is endothermic and has a very high activation free energy barrier of 5.78 eV, which can be considered as the rate-limiting step, while the formation of **4b** and **4c** is exothermic, at only -0.28 and -0.38 eV, respectively. In addition, the extremely low energy barrier for the formation of **4b** and **4c**, compared to **4a**, also further shows that His and Lys have a higher reactivity than Arg with DHA to generate colour faster. After this, the Amadori rearrangement follows to generate the Heyns product. Although this step is exothermic in all three pathways, their energy values vary greatly (-0.07, -0.28 and -6.13 eV for **5c**, **5b** and **5a**, respectively). In terms of the transformation from DHA to MGO, it undergoes an enolisation to form **1** with energy raising (ΔG=0.18 eV) and then follows by dehydration and enolization to generate **2** (ΔG=-0.70 eV) and MGO (ΔG=-0.26 eV), respectively, which steps are both exothermic. These observations are similar to those in previous theoretical and experimental kinetic studies of the Maillard reaction in food [36],[37]. The next is the aldol reaction where a water molecule is lost between MGO and the Heyns products (**5a**, **5b** and **5c**) to form **6a**, **6b**, **6c**, followed by cyclisation and dehydration to produce **7a**, **7b**, **7c** and **8a**, **8b**, **8c**, respectively. Both these reactions are energetically downhill processes, and their calculated energies are not much different, suggesting that the formation of the finial six-membered heterocyclic structure of **8** is thermodynamically favorable. In summary, the large decrease in the free energy from the reactants to products could be used to support the proposed reaction pathways.

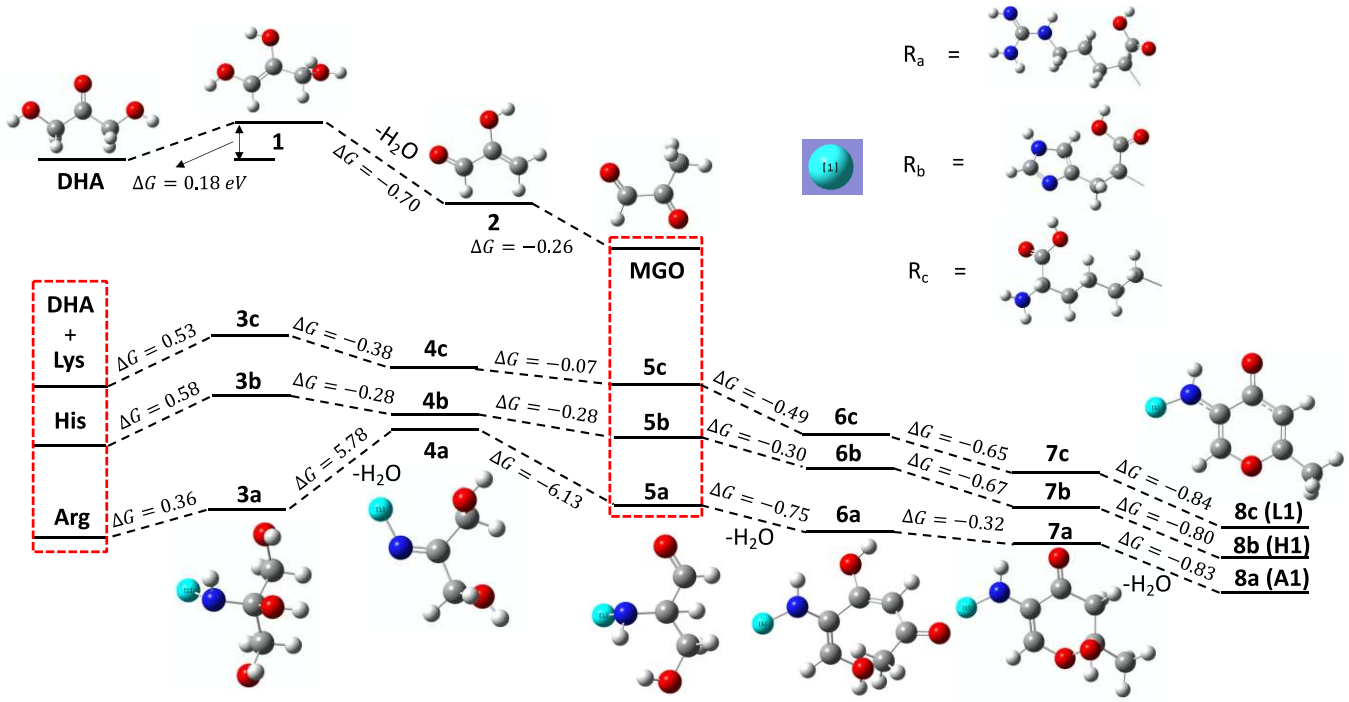

Figure 4. The variation of free energy for the proposed reactants and products during the formation of **A1**, **H1** and **L1**

3.4 Colour dilution analysis (CDA) and characterisation

Many different coloured compounds can be formed in the the Maillard reaction. To effectively identify the key coloured compounds in the Maillard reaction and rank the impact of these compounds on the colour of the complex reaction mixtures, Hofmann took a crucial step in this area by defining the colour activity value (CAV) and colour contribution (CC) [25]. However, he relied on visual assessment to determine the colour dilution factor (CDF) and the colour detection threshold (CDT) [38],[39]. Such a method could result in errors due to the limited accuracy and potential bias of human observation. To improve the accuracy and reproducibility, UV-Vis instead of a human observer was adopted to determine the CDF and CDT values. Each coloured compounds was dissolved in water to make a solution with a concentration of 3 mmol/L, which was then diluted with water repeatedly until no colour difference could be detected as indicated by the solution having the same absorbance at 420 nm as that of water.

Table 2. Colour dilution analysis and CIELAB of the key coloured compounds formed in the AA-DHA

Colourant	Conc. (mmol/L)	CDT (mmol/L)	CAV	CC (%)	*CIE*				
					*L**	*a**	*b**	*c*	*h*
A1	56.06	0.46	122	70	51.04	-0.57	15.78	15.80	92.96
H1	64.90	0.10	657	76	47.81	1.34	25.81	25.85	87.02
L1	89.57	0.14	632	77	49.28	0.84	19.55	19.57	87.53

As shown in Table 2, the lowest CDT was found for the colourant **H1** with 0.10 mmol/L (water), followed by colourant **L1** with 0.14 mmol/L. Colourant **A1** with 0.46 mmol/L showed a 4.6-fold higher detection threshold concentration. In terms of colour activity, **H1** had the highest CAV among these three colourants, with a value of 657, followed by **L1** at 632. Despite having the similar concentration as **H1**, **A1** did not have the similar CAV due to its high CDT. The calculated CAV ranked these colourants based on their relative effectiveness in generating the overall colour of the browned Maillard mixtures. The CC was used to further evaluate the percentage contribution of each colourant to the total colour.

The CC of **A1**, **H1** and **L1** was found to contribute by 70%, 76% and 77% to the total colour for Arg-DHA, His-DHA and Lys-DHA, respectively, which played a critical role in generating colour in AA-DHA reaction and they could be identified as the key colourants. Although the CC values of these three colourants were high than those of Hofmann's isolated coloured compounds from pentose-alanine reaction, they showed a similar result to Kyoko's report, where furpenthiazinate contributed about 67% of the total colour of the cysteine-furfural reaction [25],[39],[40]. In addition, these colourants were characterised using CIELAB colour space. Thus, as can be seen from Table 2, the colour characteristics of these colourants were mainly reflected in the values of b^* (yellowness). The highest b^* value was found for **H1** to be 25.81, followed by **L1** at 19.55. Colourant **A1** showed the lowest b^* value at 15.78. Meanwhile, the structural and electronic properties of **A1**, **H1** and **L1** were examined using DFT. The electron density distributions of the highest occupied molecular orbital (HOMO) and lowest unoccupied molecular orbital (LUMO) were shown in Figure 5. The energy gap ΔE (= E_{HOMO}-E_{LUMO}) could reveal the ease of electronic transition from HOMO to LUMO [41],[42]. It can be clearly seen from Figure 5 that **H1** (4.11 eV) and **L1** (4.17 eV) showed a smaller ΔE than that of **A1** (4.25 eV), indicating that **H1** and **L1** had a stronger browning intensity than **A1**, which explains the colour difference between His-DHA, Lys-DHA and Arg-DHA when the concentrations of the key colourants were similar.

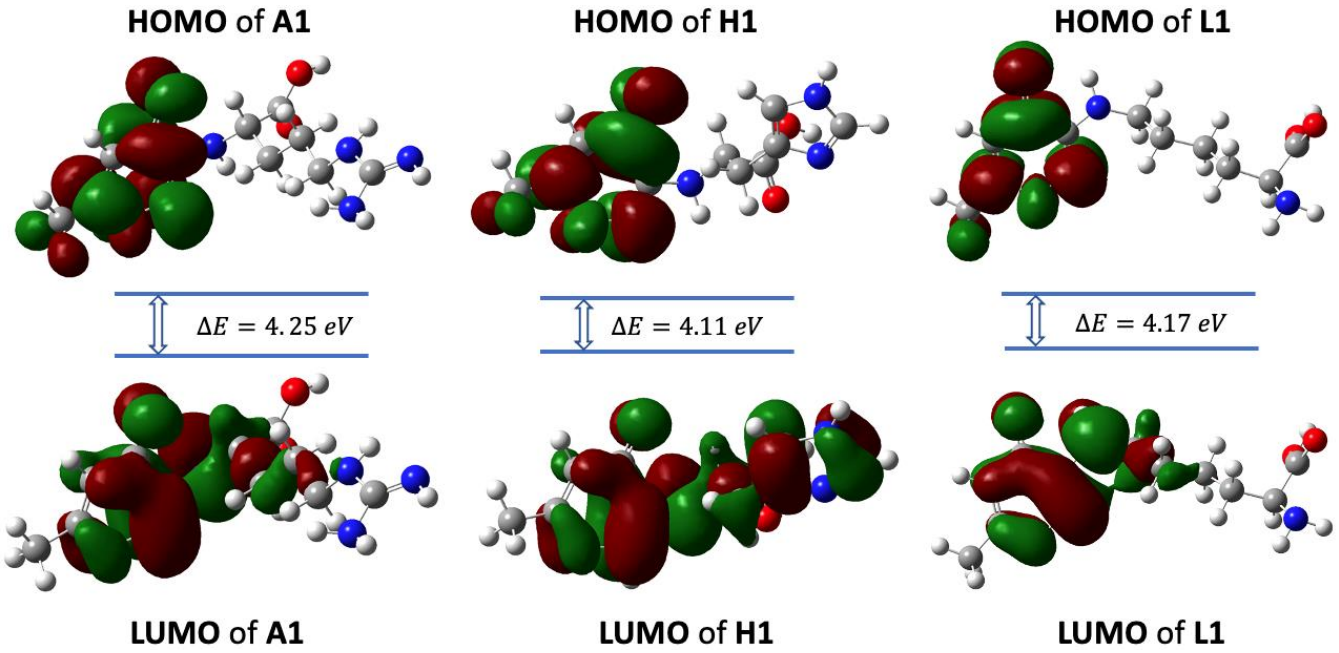

Figure 5. HOMO and LUMO of **A1**, **H1** and **L1** calculated at B3LYP at 6-311+ basis set

4. CONCLUSION

In summary, three primary key coloured compounds with the same chromophore (**A1**, **H1** and **L1**) had been successfully isolated and identified. A possible reaction pathway for the formation of these colourants had also been proposed and validated by compution. DFT results showed that the large decrease in the free energy from the reactants to products was able to support the proposed reaction pathway. The very large difference in the energy barrier for the formation of Schiff base from Arg has further shown that His and Lys have higher reactivities than Arg with DHA to generate colour faster. In addition, CDA was a powerful tool to evaluate the colour impact of colourant formed in the complex Maillard reaction mixtures. In terms of colour activity, **H1** had the highest CAV at 657, followed by **L1** at 632. **A1** had the lowest CAV at 122. The CC results showed that **A1**, **H1** and **L1** were responsible for 70%, 76% and 77% of the

total colour for Arg-DHA, His-DHA and Lys-DHA, respectively, indicating that their concentration determines the browning intensity of the AA-DHA. CIE results demonstrated that the colour characteristic of these colourants was mainly reflected in the values of b^* (yellowness). The highest b^* value was found for **H1** at 25.81, followed by **L1** at 19.55, with **A1** showing the lowest b^* value at 15.78. Meanwhile, the energy gap ΔE (= E_{HOMO}-E_{LUMO}) of **H1** (4.11 eV) and **L1** (4.17 eV) showed a smaller ΔE than that of **A1** (4.25 eV). These results indicated that **H1** and **L1** have a stronger browning intensity than **A1**, which could be used to explain the colour difference between these AA-DHA mixtures.

AUTHOR CONTRIBUTION STATEMENT

Yufa Sun: Investigation, Experimental design, Methodology, Characterization, Writing - original draft. **Peiyu Zhang**: Compound analysis, Writing – review & editing. **Xingyu Wang**: Computing, Validation, Writing – review & editing. **Fatimah A. M. Al-Zahrani**: Software. **Nora H.de Leeuw**: Date curation, Software, Writing – review & editing. **Long Lin**: Funding acquisition, Supervision, Writing – review & editing.

DECLARATION OF COMPETING INTEREST

The authors declare that they have no known competing financial interests or personal relationships that could have appeared to influence the work reported in this paper.

ACKNOWLEDGMENT

The authors would like to thank the University of Leeds for funding the study through the Leeds International Doctoral Scholarship (LIDS). Peiyu Zhang and Xingyu Wang both acknowledge the University of Leeds and the China Scholarship Council (CSC) for financial support. The authors would also like to thank Dr. Jeanine Williams for providing a lot of help and useful discussions on the separation of HPLC and the analysis of chromatography.

REFERENCES

[1] Hellwig M, Henle T. Baking, ageing, diabetes: A short history of the Maillard reaction. Angew Chemie - Int Ed 2014;53:10316–29. https://doi.org/10.1002/anie.201308808.

[2] Cui H, Yu J, Zhai Y, Feng L, Chen P, Hayat K, et al. Formation and fate of Amadori rearrangement products in Maillard reaction. Trends Food Sci Technol 2021;115:391–408. https://doi.org/10.1016/j.tifs.2021.06.055.

[3] Hodge JE. Dehydrated foods, chemistry of browning reactions in model systems. J Agric Food Chem 1953;1:928–43. https://doi.org/10.1021/jf60015a004.

[4] Steinhart H. The Maillard Reaction. Chemistry, Biochemistry and Implications. By Harry Nursten. Angew Chemie Int Ed 2005;44:7503–4. https://doi.org/10.1002/anie.200585332.

[5] Hofmann T. Studies on melanoidin-type colorants generated from the Maillard reaction of protein-bound lysine and furan-2-carboxaldehyde-Chemical characterisation of a red coloured domaine. Eur Food Res Technol 1998;206:251–8. https://doi.org/10.1007/s002170050253.

[6] Echavarría AP, Pagán J, Ibarz A. Melanoidins formed by Maillard reaction in food and their biological activity. Food Eng Rev 2012;4:203–23. https://doi.org/10.1007/s12393-012-9057-9.

[7] Somoza V, Fogliano V. 100 years of the maillard reaction: Why our food turns brown. J Agric Food Chem 2013;61:10197. https://doi.org/10.1021/jf403107k.

[8] Fisher DE, James WD. Indoor tanning - science, behavior, and policy. N Engl J Med 2010;363:901–3. https://doi.org/10.1056/NEJMp1005999.

[9] Garone M, Howard J, Fabrikant J. A review of common tanning methods. J Clin Aesthet Dermatol 2015;8:43–7.
[10] Nguyen BC, Kochevar IE. Factors influencing sunless tanning with dihydroxyacetone. Br J Dermatol 2003;149:332–40. https://doi.org/10.1046/j.1365-2133.2003.05434.x.
[11] Ricapito NG, Ghobril C, Zhang H, Grinstaff MW, Putnam D. Synthetic biomaterials from metabolically derived synthons. Chem Rev 2016;116:2664–704. https://doi.org/10.1021/acs.chemrev.5b00465.
[12] Wittgenstein E, Berry HK. Staining of skin with dihydroxyacetone. Science (80-) 1960;132:894–5. https://doi.org/10.1126/science.132.3431.894.
[13] Wittgenstein E, Berry HK. Reaction of dihydroxyacetone (DHA) with human skin callus and amino compounds. J Invest Dermatol 1961;36:283–6. https://doi.org/10.1038/jid.1961.46.
[14] Ciriminna R, Fidalgo A, Ilharco LM, Pagliaro M. Dihydroxyacetone: An updated insight into an important bioproduct. ChemistryOpen 2018;7:233–6. https://doi.org/10.1002/open.201700201.
[15] Bobin MF, Martini MC, Cotte J, Potin P. Effects of color adjuvants on the tanning effect of dihydroxyacetone. J Soc Cosmet Chem Japan 1984;35:265–72.
[16] Pantini G, Ingoglia R, Brunetta F, Brunetta A. Sunless tanning products containing dihydroxyacetone in combination with a perfluoropolyether phosphate. Int J Cosmet Sci 2007;29:201–9. https://doi.org/10.1111/j.1467-2494.2007.00381.x.
[17] Carnali JO, Madison SA, Shah P, Qiu Q. Structure/property relationship for ethylenediamine derivatives as aids in sunless tanning. Ind Eng Chem Res 2012;51:15573–81. https://doi.org/10.1021/ie301929w.
[18] Lloyd R V., Fong AJ, Sayre RM. In Vivo formation of Maillard reaction free radicals in mouse skin. J Invest Dermatol 2001;117:740–2. https://doi.org/10.1046/j.0022-202x.2001.01448.x.
[19] Jung K, Seifert M, Herrling T, Fuchs J. UV-generated free radicals (FR) in skin: Their prevention by sunscreens and their induction by self-tanning agents. Spectrochim Acta - Part A Mol Biomol Spectrosc 2008;69:1423–8. https://doi.org/10.1016/j.saa.2007.09.029.
[20] Nguyen BC, Kochevar IE. Influence of hydration on dihydroxyacetone-induced pigmentation of stratum corneum. J Invest Dermatol 2003;120:655–61. https://doi.org/10.1046/j.1523-1747.2003.12089.x.
[21] Sun Y, Lin L, Zhang P. Color development kinetics of Maillard reactions. Ind Eng Chem Res 2021;60:3495–501. https://doi.org/10.1021/acs.iecr.1c00026.
[22] Al-Zahrani FAM, Alzahrani KA, El-Shishtawy RM, Abu Mellah K, Al-Soliemy AM, Asiri AM. Synthesis, photophysical properties, and density functional theory studies of phenothiazine festooned vinylcyclohexenyl-malononitrile. Luminescence 2020;35:998–1009. https://doi.org/10.1002/bio.3804.
[23] Christie RM. Colour chemistry 2nd eddition. 2015. https://doi.org/10.1002/col.10090.
[24] Swinehart DF. The Beer-Lambert law. J Chem Educ 1962;39:333–5. https://doi.org/10.1021/ed039p333.
[25] Hofmann T. Studies on the influence of the solvent on the contribution of single Maillard reaction products to the total color of browned pentose/alanine solutions - A quantitative correlation using the color activity concept. J Agric Food Chem 1998;46:3912–7. https://doi.org/10.1021/jf980478a.
[26] Robertson AR. The CIE 1976 color-difference formulae. Color Res Appl 1977;2:7–11. https://doi.org/10.1002/j.1520-6378.1977.tb00104.x.
[27] Mottram DS, Wedzicha BL, Dodson AT. Food chemistry: Acrylamide is formed in the Maillard reaction. Nature 2002;419:448–9. https://doi.org/10.1038/419448a.

[28] Ledl F, Schleicher E. New aspects of the Maillard reaction in foods and in the human body. Angew Chemie Int Ed English 1990;29:565–94. https://doi.org/10.1002/anie.199005653.

[29] Sun Y, Liu C, Hong Y, Liu R, Zhou X. Synthesis and application of self-crosslinking and flame retardant waterborne polyurethane as fabric coating agent. Prog Org Coatings 2019;137:105323. https://doi.org/10.1016/j.porgcoat.2019.105323.

[30] Nikahd M, Mikusek J, Yu LJ, Coote ML, Banwell MG, Ma C, et al. Exploiting Chitin as a Source of Biologically Fixed Nitrogen: Formation and Full Characterization of Small-Molecule Hetero- And Carbocyclic Pyrolysis Products. J Org Chem 2020;85:4583–93. https://doi.org/10.1021/acs.joc.9b03438.

[31] Chen VJ, Minto RE, Manicke N, Smith GD. Structural elucidation of two Congo red derivatives on dyed historical objects indicative of formaldehyde exposure and the potential for chemical fading. Dye Pigment 2022;201:110173. https://doi.org/10.1016/j.dyepig.2022.110173.

[32] Wang Y, Ho CT. Flavour chemistry of methylglyoxal and glyoxal. Chem Soc Rev 2012;41:4140–9. https://doi.org/10.1039/c2cs35025d.

[33] Kanzler C, Wustrack F, Rohn S. High-Resolution Mass Spectrometry Analysis of Melanoidins and Their Precursors Formed in a Model Study of the Maillard Reaction of Methylglyoxal with <scp>l</scp> -Alanine or <scp>l</scp> -Lysine. J Agric Food Chem 2021;69:11960–70. https://doi.org/10.1021/acs.jafc.1c04594.

[34] Prabakaran K, Manivannan R, Oh H, Parthiban C, Son YA. Synthesis and characterisation of new acridine dye molecules combined UV absorber and exploring photophysical properties. Dye Pigment 2021;192:109391. https://doi.org/10.1016/j.dyepig.2021.109391.

[35] Jalbout AF, Abul Haider Shipar MD, Trzaskowski B, Adamowicz L. Formation of glyoxal in hydroxyacetaldehyde and glycine nonenzymatic browning Maillard reaction: A computational study. Food Chem 2007;103:359–68. https://doi.org/10.1016/j.foodchem.2006.07.061.

[36] Nasiri R, Field MJ, Zahedi M, Moosavi-Movahedi AA. Cross-linking mechanisms of arginine and lysine with α,β-dicarbonyl compounds in aqueous solution. J Phys Chem A 2011;115:13542–55. https://doi.org/10.1021/jp205558d.

[37] Shipar MAH. Formation of the Heyns rearrangement products in dihydroxyacetone and glycine Maillard reaction: A computational study. Food Chem 2006;97:231–43. https://doi.org/10.1016/j.foodchem.2005.03.041.

[38] Frank O, Hofmann T. Characterization of key chromophores formed by nonenzymatic browning of hexoses and L-alanine by using the color activity concept. J Agric Food Chem 2000;48:6303–11. https://doi.org/10.1021/jf0001987.

[39] Hofmann T. Characterization of the most intense coloured compounds from Maillard reactions of pentoses by application of colour dilution analysis. Carbohydr Res 1998;313:203–13. https://doi.org/10.1016/S0008-6215(98)00279-1.

[40] Noda K, Masuzaki R, Terauchi Y, Yamada S, Murata M. Novel Maillard pigment, furpenthiazinate, having furan and cyclopentathiazine rings formed by acid hydrolysis of protein in the presence of xylose or by reaction between cysteine and furfural under strongly acidic conditions. J Agric Food Chem 2018;66:11414–21. https://doi.org/10.1021/acs.jafc.8b05302.

[41] Shahab S, Hajikolaee FH, Filippovich L, Darroudi M, Loiko VA, Kumar R, et al. Molecular structure and UV–Vis

spectral analysis of new synthesized azo dyes for application in polarizing films. Dye Pigment 2016;129:9–17. https://doi.org/10.1016/j.dyepig.2016.02.003.

[42] Wu Y, Gui H, Ma L, Zou L, Ma X. Red-light emissive phosphorescent polymers based on X-shaped single benzene. Dye Pigment 2022;198:110005. https://doi.org/10.1016/j.dyepig.2021.110005.